Arch Environ Contam Toxicol (2010) 59:393–406
DOI 10.1007/s00244-010-9501-x

Role of Lactone Ring in Structural, Electronic, and Reactivity Properties of Aflatoxin B1: A Theoretical Study

Inés Nicolás-Vázquez · Abraham Méndez-Albores · Ernesto Moreno-Martínez · René Miranda · Miguel Castro

Received: 19 October 2009 / Accepted: 9 March 2010 / Published online: 26 March 2010

Abstract This study involved quantum mechanical calculations to explain the chemical behavior of the lactone ring of aflatoxin B1, which is a carcinogenic hazardous compound. The aflatoxin B1 compound, produced by the fungi *Aspergillum flavus*, was studied with the B3LYP/6-311+G(d,p) method; its reactivity properties were accounted for by means of the calculated geometrical and electronic parameters. The results obtained indicate that the fused A, B, C, and D rings of aflatoxin adopt a continuous planar conformation. The carbon atom of the lactone group presents a highly electrophilic character, since the population analysis yields a high positive charge for this atom, whereas high negative charges were recorded for both oxygen sites of that group. Thus, in an acidic aqueous medium, the oxygen atoms could be protonated and the carbon site may suffer a nucleophilic attack by water. Accordingly, the OC−O bond length has been lengthened substantially. So it was demonstrated that the lactonic ring of aflatoxin B1 is hydrolyzed under acidic conditions by an acid-acyl bimolecular mechanisms, $A_{AC}2$, suggesting the deletion of its carcinogenic properties.

Aflatoxins are a group of acutely toxic metabolites produced by toxigenic strains of fungi such as *Aspergillus flavus* Link and *Aspergillus parasiticus* Speare (Asao et al. 1963). These toxins have closely similar structures and form a unique group of highly oxygenated, naturally occurring heterocyclic compounds. Four principal aflatoxins (AFs) are produced by this fungus: AFB_1, AFB_2, AFG_1, and AFG_2. AFB_1 is considered among the most powerful hepatocarcinogenic agents known. In 1987 the International Agency for the Investigation in Cancer stated that aflatoxins represent a high potential risk for cancer in humans (IARC 1987). Contamination of foods and feedstuffs with aflatoxins is a serious problem for human and animal health. Many experiments have therefore been performed to reduce the level of aflatoxins in contaminated crops (Mercado et al. 1991; Samarajeewa et al. 1991). The aim of these methods is either to remove or to destroy the toxin from food or feed, and they can be classified into chemical, biological, and physical methods.

A large number of chemicals can react with aflatoxins and convert them to less toxic and mutagenic compounds. These chemicals include acids (Buchi et al. 1967; Dutton and Heathcote 1968), bases (Dollear et al. 1968; Mann et al. 1970; Park et al. 1981, 1984, 1988), oxidizing agents (Cater et al. 1974; Applebaum and Marth 1982; McKenzie et al. 1997, 1998), bisulfites (Doyle and Marth 1978a, b; Moerck et al. 1980; Hagler et al. 1982, 1983), and gases (Brekke et al. 1978; Samarajeewa et al. 1991). However, most of the chemical processes that have been investigated

Electronic supplementary material The online version of this article (doi:10.1007/s00244-010-9501-x) contains supplementary material, which is available to authorized users.

I. Nicolás-Vázquez (✉) · A. Méndez-Albores · E. Moreno-Martínez · R. Miranda
Departamento de Ciencias Químicas, Campo 1, Facultad de Estudios Superiores Cuautitlán, Universidad Nacional Autónoma de México, Cuautitlán Izcalli, C.P. 54740 Estado de México, Mexico
e-mail: nicovain@yahoo.com.mx

M. Castro (✉)
Departamento de Física y Química Teórica, DEPg. Facultad de Química, Universidad Nacional Autónoma de México, Del. Coyoacán, C.P. 04510 México D.F., Mexico
e-mail: castro@quetzal.pquim.unam.mx

are impractical (required to be carried out under extreme conditions of temperature and pressure), are unsafe (due to the formation of toxic residues), and compromise the nutritional, sensory, and functional properties of the product. Currently, ammoniation and treatment with sodium bisulfite are the major industrial processes most widely used to inactivate aflatoxins in peanut meal, maize, and cottonseed destined for animal feeding.

Our previous studies have shown that certain organic acids perform a detoxification function in treating aflatoxin-contaminated commodities, providing certain protection to ducklings from aflatoxin toxicity and reducing the mutagenic activity of aflatoxins in the *Salmonella* microsomal screening system (Méndez-Albores et al. 2005, 2007).

These results suggest that detoxification of AFB_1 initially involves the formation of a β-keto acid structure (catalyzed by the acidic medium), followed by hydrolysis of the lactone ring, yielding aflatoxin D_1 (AFD_1), derived from decarboxylation of the lactone ring-opened form AFB_1, which is 450 times less mutagenic than AFB_1 and presents an 18-fold toxicity decrease (Méndez-Albores et al. 2008; L. Lee et al. 1981). Although x-ray and nuclear magnetic resonance spectra of the AFB1 molecule have been reported (van Soest and Peerdeman 1970a, b), there is no specific information available concerning the structural and electronic parameters of the lactonic ring in the aflatoxin molecule. As far as we know, there are few theoretical studies of this compound (Pachter and Steyn 1985; Pavão et al. 1995; Okajima and Hashikawa 2000; Billes et al. 2006; Yiannikouris et al. 2006; Bren et al. 2007; Ramírez-Galicia et al. 2007), and they do not address the importance of the lactonic ring in the reactivity properties of AFB1. Consequently, the purpose of the present research deals with determination of the structural and electronic properties of the lactonic ring of the aflatoxin B1 compound, particularly when the lactonic ring suffers a rupture induced by the aqueous acid medium (Scheme 1). This study is realized by means of theoretical calculations, using density functional theory (DFT)-based methods and supercomputer facilities.

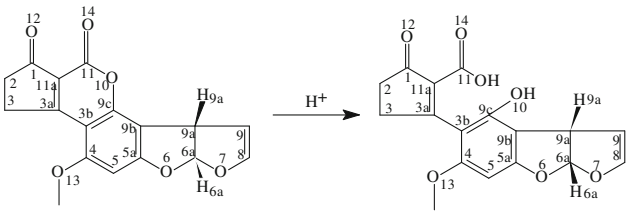

Scheme 1 Rupture of the lactonic ring, promoted by the aqueous acid medium

Computational Methodology

In the first step, the target molecule was built with standard bond lengths and bond angles, using the PC Spartan 02 program (Deppmeier et al. 2002). The connectivity frame of this compound suggests four possible stereoisomers (Fig. 1a), because both H_{9a} and H_{6a} of the C_{9a} and C_{6a} centers can be on the same side, either the front, yielding structure **1**, or back and front, yielding structure **2**. In addition, there are alternate configurations: H_{6a} in front and H_{9a} in back (**3**) and the inverse structure (**4**). Therefore, the first task was to establish the conformation of maximum stability. Thus, the geometry for each stereoisomer was fully optimized using the AM1 (Dewar et al. 1985) semi-empirical method implemented in Spartan 02. Furthermore, DFT calculations were carried out using the Gaussian 03 (Frisch et al. 2003) program at the level of theory defined by the hybrid Becke's three-parameter hybrid functional, B3LYP (Becke 1988, 1993; Lee et al. 1988), which includes a mixture of Hartree–Fock exchange with DFT exchange correlation, has been employed. The basis set used includes the split-valence basis sets of 6-31G(d,p) (Hariharan and Pople 1973). Also, a diffuse function 6-311+G(d,p) (Clark et al. 1983; Frisch et al. 1984) was used. The default convergence criteria were also employed.

Then the optimized geometries for the ground and higher-energy states were determined with the B3LYP/6-31G(d,p) and B3LYP/6-311+G(d,p) methods. The minima were verified by performing a vibrational analysis with these methods. The structural parameters (bond lengths, bond angles, dihedral angles), natural atomic charges, electrostatic potential molecular surfaces, HOMO (lowest occupied molecular orbital), and LUMO (lowest unoccupied molecular orbital) were used to analyze the electrophilic or nucleophilic character, which can be involved in the reactivity of the aflatoxin B1 compound. These properties were analyzed at the B3LYP/6-311+G(d,p) level.

The bond orders were calculated for the B3LYP/6-31G(d,p) optimized structure of stereoisomer **1**. We have proposed a mechanism for B1 (**1**) with an acidic treatment, to explain the formation of a compound that contains both hydroxyl and carboxylic groups. Also, we performed gas-phase geometry optimization employing the 6-311+G(d,p) basis set, for intermediates and transition states (TSs) of **1**, which were confirmed by frequency calculations at the same level of theory. In all cases intrinsic reaction coordinate (IRC) calculations were performed to test whether the determined TSs connect with the proper reactants and products.

Absorption spectra determining vertical electronic excitations from the ground state using the TD-DFT method implemented in Gaussian 03, B3LYP/6-31G(d,p),

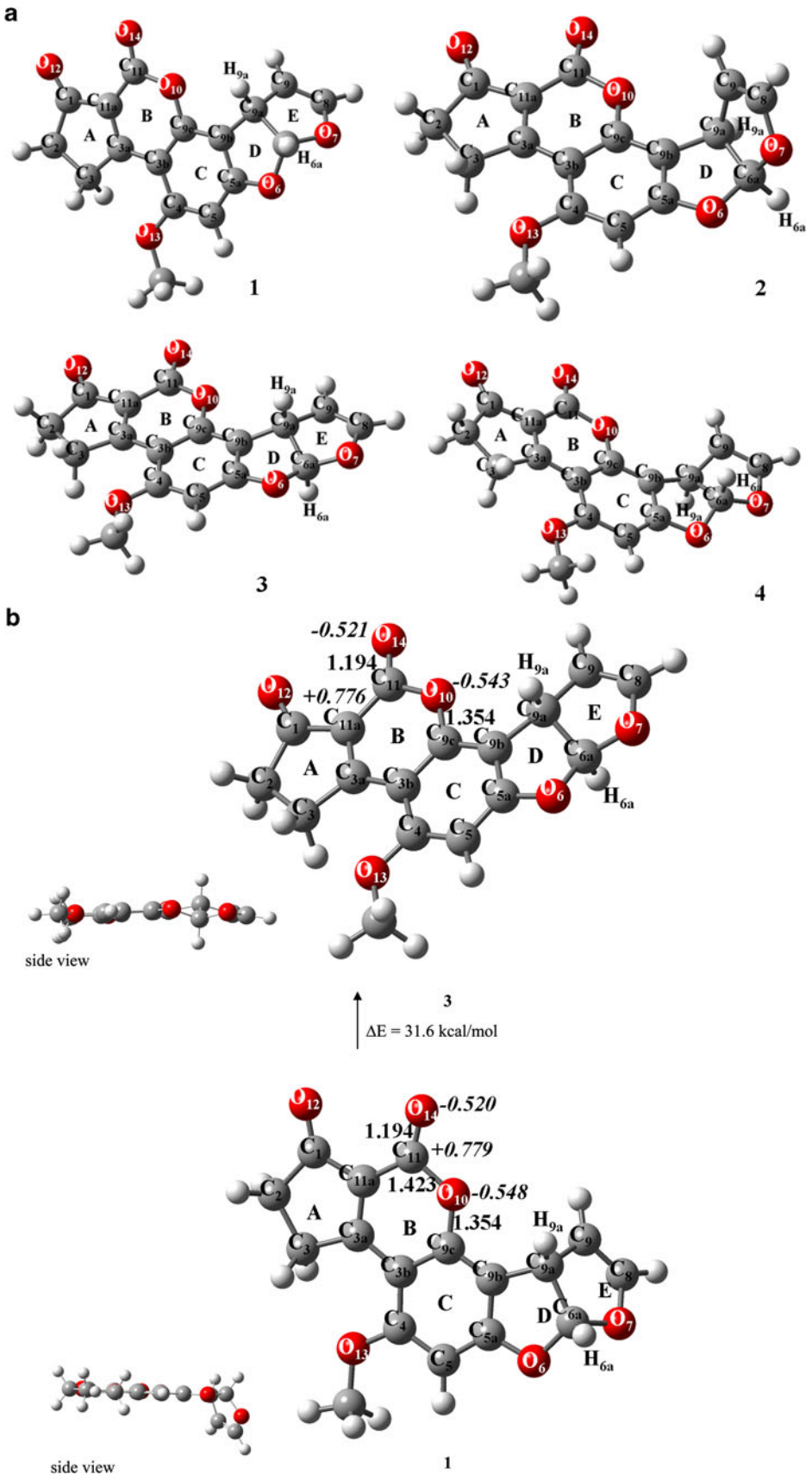

Fig. 1 **a** Four possible stereoisomers of the aflatoxin molecule, both H_{9a} and H_{6a} of the C_{9a} and C_{6a} centers, can be on the same side, either the front, yielding structure **1**, or the back, yielding structure **2**. Or they can lie in an alternate pattern: H_{6a} in front and H_{9a} in back (**3**) or the inverse (**4**). **b** Selected geometrical parameters of the B3LYP/6-311+G(d,p) optimized structures, 1 and 3. Bond lengths are given as angstroms, and the atomic charges for some selected atoms (electron units; boldface) determined in the natural population analysis are indicated

were used (Stratmann et al. 1998; Maitra and Tempel 2006).

Results and Discussion

Ground State of Aflatoxin B1

As stated above, in the first phase of this study the four stereoisomers **1**–**4** of aflatoxin B1 were fully optimized using semiempirical calculations at the AM1 level, with the observation that the hydrogen atoms can lie on the same side, originating structures **1** and **2**, with the same estimation for the formation energy of 138.3 kcal/mol. As shown in Fig. 1a, when these hydrogen atoms are in alternating fashion structures **3** and **4** are formed, with a considerably lower formation energy, 89.8 kcal/mol (Supplementary Table 1S). That is, **3** and **4**, are located, with respect to **1** and **2,** at a significant higher energy, 48.5 kcal/mol, also indicating the strong structural and energetic effects produced by the H atoms lying alternately or on the same side. As shown in Fig. 1a, in the ground-state structure the A, B, C, and D rings are in-plane, whereas in structure **3**, all the rings tend to be on-plane, but the E ring is strongly distorted or stressed. These results indicate that the presence of **3** and **4** in a given sample may be disregarded.

Although the geometric parameters can be reasonably predicted by the semiempirical AM1 method, frequently this approach yields an incorrect electronic structure. For these reasons, the already located **1**–**4** structures were reoptimized at a higher level of theory, using DFT-based-methods. In particular, the B3LYP functional and the 6-31G(d,p) and 6-311+G(d,p) basis sets were used. DFT calculations were done with the Gaussian 03 program.

The results obtained confirmed that **1** and **2** are the lowest-energy states, since **3** and **4** were located 31.6 kcal/mol higher in energy, at the B3LYP/6-311+G(d,p) level, or 31.9 kcal/mol using B3LYP/6-31G(d,p) (see Fig. 1b). Moreover, the vibrational analysis performed indicated that **1** and **2** are true minima on the potential energy surface, since real frequencies were obtained for these structures.

On the other hand, and according to the literature, the x-ray results (van Soest and Peerdeman 1970a, b) have revealed that the ground-state structure of the aflatoxin B1 compound corresponds when the hydrogen atoms are located on the same side of the molecular plane, in agreement with our theoretical results. The lowest-energy structure of aflatoxin, **1,** is shown in Fig. 1b. It is worth mentioning that AM1 produces an average deviation of 0.018 Å for the equilibrium bond lengths, while this deviation is 0.015 and 0.014 Å for the B3LYP/6-31G(d,p) and B3LYP/6-311+G(d,p) methods. At the latter level of description, the two carbonyl groups, C_1-O_{12} and $C_{11}-O_{14}$, in rings A and B have negative charges on the oxygen centers, implying repulsion between these oxygen centers (see structure **1** in Fig. 1b), which are separated by 3.10 Å; note that the A and B rings are rigid. Smaller repulsion is expected for the O_6 and O_7 centers, which have negligible negative charges and a separation of 2.35 Å. Considering the large number of their geometric parameters we present only their bond lengths (Table 1), their valence angles (Table 2), and some dihedral angles (Table 3). Then the average deviations of the bond lengths obtained with split-valence basis sets using the B3LYP functional are closer to the experimental values; see Table 1. Note that the equilibrium bond lengths for the C ring, 1.39 Å, fall in the regime of double-bond formation, suggesting an aromatic behavior. Moreover, C is conjugated with the B cycle, which, together with their planarity, as stated above, originates fluorescence. This phenomenon is discussed below.

Considering the almost-planar geometry of the aflatoxin molecule, as well as the rupture of the lactonic ring under acidic conditions; it is necessary to realize other theoretical studies supporting this behavior. Therefore, bond orders, charges, map of electrostatic potential, HOMO, and LUMO, as well as some key steps in the hydrolysis reaction and fluorescence, were also determined.

Bond Orders

The triplet state is promoted by light in the 425-nm region (Purchase 1974) and plays an important role in fluorescence behavior and in the reactivity properties of the aflatoxin compound. Therefore, we proceed with the estimation of the bond orders (Mayer 1986a, b) for both the ground state and the higher-energy triplet state. The results are reported in Table 4; the differences between these states are also indicated. The objective is to examine whether the excited triplet state presents significant differentiation in terms of bond length and bond order. The C_4-C_{3b}, $C_{3b}-C_{9c}$, and $C_{9b}-C_{5a}$ distances are clearly lengthened with respect to the ground state. A similar behavior occurs for the $C_{3a}-C_{11a}$, $C_{11}-O_{14}$, and $O_{10}-C_{9c}$ bonds on the B ring, which is the main active region of aflatoxin B1. Note also the observed shortening of the C_4-C_5, $C_{9b}-C_{9c}$, $C_{11a}-C_{11}$, $C_{11}-O_{10}$, and $C_{3a}-C_{3b}$ bond lengths. The bond lengths and bond orders are reported in Tables 1 and 4, for both singlet and triplet species; they clearly indicate a conjugation on benzene ring C and a considerable relaxation in the lactonic group. These results also suggest some conjugation on the lactonic ring B, contributing to the stability of aflatoxin B1. The data also show that the main difference lies in the bonds involving the central benzene ring C of aflatoxin B1. Consequently, the bond order is smaller for the $C_{11}-O_{10}$ bond, which is

Table 1 Optimized bond lengths (Å) for aflatoxin B1 (**1a–1h** and **3)** molecules at the levels of theory B3LYP/6-311+G(d,p) and the higher-energy triplet state of **1** (**1aT**)[a]

Bond	Exp.	AMI	B3LYP: 6-31G(d,p)	Molecule									
				1a	**3**	**1aT**	**1b**	**1c**	**1d**	**1e**	**1f**	**1g**	**1h**
C_1–C_{11a}	1.457	1.477	1.481	1.481	1.483	1.460	1.494	1.458	1.525	1.451	1.506	1.504	1.491
C_1–O_{12}	1.193	1.227	1.214	1.209	1.208	1.221	1.201	1.220	1.198	1.229	1.204	1.202	1.209
C_{3a}–C_{11a}	1.371	1.376	1.374	1.373	1.372	1.450	1.402	1.391	1.419	1.370	1.408	1.360	1.358
C_{11a}–C_{11}	1.455	1.438	1.451	1.449	1.451	1.445	1.384	1.384	1.354	1.445	1.395	1.448	1.475
C_{11}–O_{10}	1.415	1.414	1.421	1.423	1.420	1.412	1.462	1.319	2.294	1.566	2.737	4.637	3.328
C_{11}–O_{l4}	1.186	1.225	1.201	1.194	1.194	1.200	1.228	1.293	1.138	1.311	1.309	1.196	1.336
O_{10}–C_{9c}	1.372	1.368	1.356	1.354	1.354	1.371	1.407	1.390	1.355	1.421	1.360	1.360	1.356
C3a–C3b	1.424	1.426	1.433	1.431	1.434	1.385	1.421	1.403	1.417	1.429	1.426	1.478	1.475
C3b–C_{9c}	1.398	1.427	1.423	1.421	1.422	1.448	1.430	1.439	1.447	1.424	1.441	1.422	1.419
C_{9c}–C_{9b}	1.387	1.392	1.385	1.384	1.383	1.364	1.359	1.365	1.368	1.366	1.375	1.383	1.390
C_{9b}–C_{5a}	1.381	1.416	1.389	1.386	1.405	1.416	1.409	1.404	1.401	1.405	1.398	1.394	1.383
C_{5a}–C_5	1.401	1.392	1.396	1.393	1.389	1.391	1.390	1.397	1.388	1.388	1.389	1.390	1.389
C4–C5	1.358	1.401	1.395	1.392	1.394	1.387	1.394	1.387	1.389	1.395	1.389	1.396	1.395
C3b–C4	1.419	1.420	1.430	1.429	1.427	1.469	1.443	1.441	1.463	1.433	1.449	1.429	1.421
C_4–O_{l3}	1.358	1.375	1.357	1.355	1.355	1.353	1.333	1.337	1.334	1.340	1.340	1.354	1.365

[a] From van Soest and Peerdeman (1970b)

important for the breaking of this bond during the acidic hydrolysis. In fact, this C–O bond suffers a rupture in several types of hydrolysis. On the other hand, the calculated bond length for $O_{10}-C_{9c}$ is relatively small, with a big bond order. Therefore, these bond order and bond lengths results suggest that bond breaking is more likely to occur at the $C_{11}-O_{10}$ bond.

Charges

Figure 1b and Table 5 report the natural population analysis (Reed et al. 1985) of the atomic charges for some selected atoms of aflatoxin B1, obtained with B3LYP/6-311+G(d,p). These values indicate that the O_{10} atom is slightly more negative than the O_{14} center. Thus, the addition of a proton may occur on the O_{10} or O_{14} atoms. The total energy results indicate that the addition at O_{14} is favored, because it is 25.3 kcal/mol (relative electronic energy), more stable than the addition at the O_{10} atom. The charges for the excited molecule, listed in Table 5, also were calculated with the B3LYP/6-311+G(d,p) method. The changes in charge distribution between the ground and the excited triplet state gave an indication of the fluorescent ability of the molecule.

The charge difference between the excited and the ground state is also tabulated in Table 5. It is evident that an increase in electron charge is observed for the C_1, C_{3a}, O_{10}, and C_{11} atoms, whereas a decrease was found for O_{12} and O_{14}, with the excitation. These results indicate that the charge at both carbon, C_{11}, and oxygen, O_{14}, atoms must participate in the C=O bond, showing a small, but significant, increase in C=O bond length, from 1.194 Å in the ground state up to 1.200 Å in the excited state. Up to this point, these results allow a characterization of the structural and electronic details of the lactonic region, which is important in the hydrolysis reaction.

On the other hand, with respect to the excited state, the C_4 and C_{5a} atoms of the benzene ring show an increase in their atomic charges, whereas the atomic populations in O_{13} and C_{5a} are decreased; these changes were reflected in the slight shortening of the C_4-C_5 and C_5-C_{5a} bond lengths. Most of the electron charge in the excited state is localized in the lactonic ring, as well as in some carbon atoms of the benzene ring. These results are in agreement with the experimental observation that the phenomenon of fluorescence disappeared when aflatoxin B1 was submitted to an acid hydrolysis process (Méndez-Albores et al. 2008).

Molecular Electrostatic Potential Surfaces

As mentioned before, the electrostatic potential has been primarily used to predict sites and relative reactivities toward electrophilic or nucleophilic attacks (Murray and Politzer 1998, Murray et al. 1998, 1999). From these molecular electrostatic potential surfaces (MEPSs) it was possible to identify that aflatoxin B1 has several possible sites for an electrophilic attack. The most negative values for MEPSs were found between O_{12}, O_{14}, and O_{10}; in this sense the O_{14} position is more favorable for electrophilic attack (see Fig. 2), since the carbonylic oxygen atom of the

Table 2 Optimized bond angles (degrees) for aflatoxin B1 (**1a–1h** and **3**) molecules at the levels of theory B3LYP/6-311+G(d,p) and the higher-energy triplet state of **1** (**1aT**)[a]

Angle bond	Exp.	AMI	B3LYP: 6-31G(d,p)	Molecule									
				1a	**3**	**1aT**	**1b**	**1c**	**1d**	**1e**	**1f**	**1g**	**1h**
O_{12}–C_1–C_{11a}	129.7	128.3	128.2	128.3	128.3	127.9	126.3	123.4	126.0	123. 7	127.1	126.7	127.0
C_3–C_{3a}–C_{11a}	110.8	111.5	111.2	111.2	111.2	109.5	108.9	108.7	106.5	109.0	108.1	110.9	110.6
C_1–C_{11a}–C_{3a}	112.7	110.7	111.3	111.2	111.2	111.2	112.2	113.3	112.4	112.0	110.7	111.1	111.2
C_1–C_{11a}–C_{11}	124.8	127.5	125.5	125.7	125.6	126.1	127.2	124.3	112.7	120.5	121.0	121.3	122.1
C_{3a}–C_{11a}–C_{11}	122.4	121.8	123.2	123.1	123.2	123.1	120.5	122.4	134.9	125.8	127.4	127.6	126.7
C_3–C_{3a}–C_{3b}	128.0	127.7	127.9	127.7	127.8	131.5	127.5	132.8	123.6	129.2	123.2	121.3	119.2
C_{11a}–C_{3a}–C_{3b}	121.2	120.9	120.9	121.1	121.0	118.9	123.6	118.6	129.9	121.3	128.5	127.7	130.2
C_{11a}–C_{11}–O_{14}	128.8	133.2	129.4	129.8	129.5	128.7	144.6	124.4	165.6	118.0	119.2	130.0	113.4
C_{11a}–C_{11}–O_{10}	116.5	117.3	113.8	113.7	113.7	114.8	114.6	120.3	92.9	110.9	79.5	49.6	76.5
O_{14}–C_{11}–O_{10}	114.7	109.6	116.7	116.6	116.7	116.5	100.8	115.2	101.4	112.2	116.9	168.1	169.0
C_{11}–O_{10}–C_{9c}	122.3	120.5	123.6	123.9	123.9	123.0	126.9	120.5	121.6	120.8	103.4	66.5	88.5
O_{10}–C_{9c}–C_{9b}	115.0	117.1	116.8	116.8	116.8	117.0	120.4	116.6	121.0	115.9	120.7	123.0	117.4
O_{10}–C_{9c}–C_{3b}	122.9	123.1	122.3	122.2	122.2	122.0	114.6	121.2	116.6	121.1	118.3	116.4	123.1
C_{3b}–C_{9c}–C_{9b}	122.1	119.9	120.9	121.0	121.0	120.9	125.0	122.2	122.4	123.1	120.8	120.6	119.4
C_{3a}–C_{3b}–C_{9c}	116.5	116.5	116.1	116.1	125.8	118.1	119.1	117.0	122.0	116.8	122.1	120.4	122.1
C_{3a}–C_{3b}–C_4	125.8	124.6	126.0	126.1	125.8	125.9	125.2	125.4	122.7	124.5	121.0	120.6	119.2
C_4–C_{3b}–C_{9c}	117.7	118.9	117.9	117.9	118.2	116.0	115.6	117.5	115.3	116.8	121.0	118.1	118.3
C_{3b}–C_4–O_{13}	113.7	115.2	115.6	115.8	115.9	113.4	115.7	114.9	116.5	115.4	115.4	115.3	115.1
O_{13}–C_4–C_5	123.4	122.8	122.8	122.7	122.5	123.9	123.2	124.3	121.3	123.3	122.2	123.1	122.5
C_{3b}–C_4–C_5	123.0	122.1	121.6	121.5	121.6	122.7	121.1	120.8	122.2	121.4	122.4	121.6	122.4
C_4–C_5–C_{5a}	115.5	116.9	117.2	117.3	117.3	117.3	118.4	117.9	118.0	117.8	117.2	117.2	116.6
C_5–C_{5a}–O_6	122.4	123.4	123.0	123.0	123.7	124.4	123.2	122.6	123.2	123.3	123.0	122.9	123.3
C_5–C_{5a}–C_{9b}	115.9	123.5	123.7	123.7	123.7	122.9	123.8	124.2	123.3	123.6	123.5	123.7	123.2
C_{9b}–C_{5a}–O_6	111.8	113.1	113.3	113.3	113.3	112.7	113.0	113.2	113.5	113.1	113.5	113.4	120.0
C_{5a}–C_{9b}–C_{9c}	115.9	118.8	109.1	118.6	118.2	120.1	116.1	117.4	118.8	117.4	119.4	118.8	120.0
C_{9c}–C_{9b}–C_{9a}	134.1	132.0	132.2	132.2	136.3	131.4	135.0	133.7	132.6	133.9	132.1	132.5	131.0
C_{5a}–C_{9b}–C_{9a}	109.8	109.2	109.1	109.1	104.4	108.4	108.8	108.8	108.5	108.7	108.4	108.6	108.9

[a] From van Soest and Peerdeman (1970b)

Table 3 Optimized dihedral angles (degrees) for aflatoxin B1 (**1a–1h** and **3**) molecules at the levels of theory B3LYP/6-311+G(d,p) and the higher-energy triplet state of **1** (**1aT**)[a]

Dihedral angle	B3LYP: 6-31G(d,p)	Molecule									
		1a	**3**	**1aT**	**1b**	**1c**	**1d**	**1e**	**1f**	**1g**	**1h**
$C_1C_{11a}C_{3a}C_3$	0.0	0.1	−0.2	0.7	0.7	−0.1	−1.6	−11.5	−12.8	0.5	−0.8
$C_{11}C_{11a}C_{3a}C_3$	−179.8	−179.8	179.5	−179.2	178.5	−179.7	175.6	−176.8	156.5	−177.5	179.9
$C_{11}C_{11a}C_{3a}C_{3b}$	0.2	0.2	−0.6	0.6	−0.4	0.3	−4.2	−4.2	−29.0	6.7	1.8
$C_{11}O_{10}C_{9c}C_{3b}$	0.3	0.4	−1.2	1.1	8.9	0.5	10.3	1.2	32.9	−153.1	−35.2
$C_{11}O_{10}C_{9c}C_{3b}$	−179.6	−179.5	179.1	−179.1	−172.7	0.5	−170.8	−178.8	−151.0	25.1	148.6
$C_{9c}C_{3b}C_4C_5$	0.3	0.4	−0.6	0.9	0.6	0.5	−0.1	−0.5	0.2	1.7	2.0
$C_{9c}C_{9b}C_{5a}C_5$	−0.7	−0.3	1.3	0.1	0.5	0.1	0.4	0.2	0.7	−0.5	−0.1
$C_{9c}C_{9b}C_{5a}O_6$	−179.8	−179.5	−178.5	−178.6	−179.0	−179.2	−178.7	−178.9	−178.4	−179.1	179.3
$O_{12}C_1C_{11a}C_{3a}$	−179.9	−180.0	−180.0	−179.6	178.5	−179.8	176.8	−161.9	−179.1	179.7	177.7
$O_{14}C_{11}C_{11a}C_{3a}$	179.6	179.5	−178.8	179.2	−172.3	179.7	−173.3	144.0	169.8	−163.0	132.6
$O_{14}C_{11}O_{10}C_{9c}$	−179.8	−179.9	179.7	179.8	168.2	179.9	165.4	−145.1	−179.9	160.4	−86.7

Table 4 Bond orders for aflatoxin B1 (**1a**) molecules at the level of theory B3LYP/6-31G(d,p) and the higher-energy triplet state of **1** (**1aT**)

Bond order	**1a**	**1aT**	Difference: excited – ground
C_1–C_2	0.941	0.947	0.006
C_1–C_{11a}	0.983	1.059	0.076
C_1–O_{12}	1.885	1.783	−0.102
C_3–C_{3a}	1.013	1.002	−0.011
C_{3a}–C_{11a}	1.497	1.079	−0.418
C_{11a}–C_{11}	1.035	1.044	0.009
C_{11}–O_{10}	0.850	0.877	0.027
C_{11}–O_{14}	1.922	1.873	−0.049
O_{10}–C_{9c}	0.956	0.897	−0.058
C_{3a}–C_{3b}	1.163	1.383	0.219
C_{3b}–C_{9c}	1.225	1.121	−0.104
C_{9c}–C_{9b}	1.366	1.490	0.124
C_{9b}–C_{5a}	1.354	1.205	−0.149
C_{9b}–C_{9a}	0.932	0.934	0.002
C_{5a}–C_5	0.882	1.329	0.447
C_4–C_5	1.354	1.378	0.024
C_{3b}–C_4	1.256	1.114	−0.142
C_4–O_{13}	0.944	0.945	0.001
C_{5a}–O_6	0.914	0.901	−0.012
O_6–C_{6a}	0.882	0.880	−0.002
C_{6a}–C_{9a}	0.948	0.947	−0.002
C_{9a}–C_9	0.994	0.992	−0.001
C_8–C_9	1.841	1.834	−0.007
C_8–O_7	0.955	0.956	0.001
O_7–C_{6a}	0.947	0.946	0.000

lactonic moiety, O_{14}, is the site with the largest negative potential, indicating the highest nucleophilic character of this atom. The sites with a positive potential are scattered among the different hydrogen atoms, C_{6a}, C_8, and the hydrogen atoms of the methyl group, CH_3O_{13}. According to the reaction conditions, these positive centers are not feasible for a nucleophilic attack. On the other hand, the natural population analysis indicated a strong deficiency of electron density on the C_{11} carbon atom, due to the oxygen atom O_{14}, which polarizes the C_{11} carbon atom.

In general, nucleophilic attacks on target molecules could occur at positive sites, and an electrophilic procedure should occur at the negative sites of aflatoxin B1. The electrostatic potential is a useful expression of this idea.

HOMO and LUMO Localizations

The contour plots of the HOMO and LUMO frontier orbitals were obtained with the B3LYP/6-311+G(d,p) method. As shown in Fig. 3, HOMO is mainly localized on the O_{12} and O_{14} sites; also, some π-bond contributions are recorded on ring C. In other words, HOMO has strong contributions from "*p*" orbitals, as can be appreciated in the carbon atoms of the title molecule; this charge distribution is additional to the lone electron pairs of the named oxygen atoms. Therefore, HOMO indicates the regions with a more Lewis-base character of aflatoxin B1. Due to the low reactivity of a π-bond with a proton under the experimental conditions previously stated, the major Lewis-basic sites correspond to O_{12} and O_{14}. A similar pattern was observed for the HOMO-1 and HOMO-2

Table 5 Calculated B3LYP/6-311+G(d,p) natural population analysis of the atomic charges (e^-) of some atoms for aflatoxin B1 (**1a–1h** and **3**) molecules and the higher-energy triplet state of **1** (**1aT**), as well as their difference (excited state [**1aT**] − ground state [**1a**])

Atom	Molecule										
	1a	**3**	**1aT**	**1aT – 1a**	**1b**	**1c**	**1d**	**1e**	**1f**	**1g**	**1h**
O_{10}	−0.548	−0.543	−0.570	−0.022	−0.576	−0.438	−0.671	−0.579	−0.671	−0.665	−0.716
O_{12}	−0.533	−0.533	−0.514	0.019	−0.493	−0.565	−0.560	−0.592	−0.513	−0.506	−0.547
O_{13}	−0.540	−0.539	−0.521	0.019	−0.517	−0.521	−0.520	−0.526	−0.525	−0.553	−0.554
O_{14}	−0.528	−0.521	−0.497	0.031	−0.531	−0.581	−0.347	−0.677	−0.584	−0.538	−0.534
C_1	0.552	0.554	0.488	−0.064	0.569	0.574	0.746	0.572	0.568	0.573	0.564
C_{3a}	0.130	0.140	−0.084	−0.214	0.191	0.188	0.161	0.177	0.236	0.170	0.130
C_{3b}	−0.231	−0.246	−0.080	0.151	−0.197	−0.184	−0.202	−0.214	−0.222	−0.199	−0.116
C_4	0.407	0.397	0.374	−0.033	0.448	0.425	0.447	0.436	0.438	0.351	0.351
C_5	−0.353	−0.355	−0.339	0.014	−0.332	−0.322	−0.350	−0.330	−0.348	−0.359	−0.361
C_{5a}	0.385	0.381	0.342	−0.043	0.430	0.431	0.441	0.415	0.428	0.400	0.370
C_{9b}	−0.182	−0.208	−0.148	0.034	−0.135	−0.128	−0.167	−0.137	−0.182	−0.176	−0.158
C_{9c}	0.492	0.569	0.469	−0.023	0.384	0.389	0.409	0.371	0.412	0.355	0.363
C_{11}	0.779	0.776	0.744	−0.035	0.815	0.814	0.911	0.872	0.828	0.825	0.822
C_{11a}	−0.285	−0.285	−0.120	0.165	−0.312	−0.322	−0.389	−0.318	−0.318	−0.300	−0.278

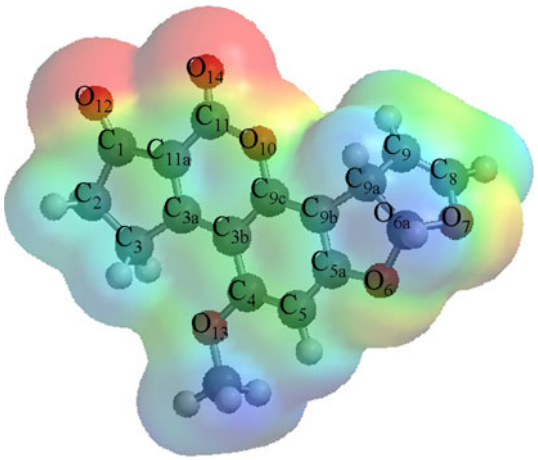

Fig. 2 Electrostatic potential molecular surface of **1a**

orbitals, which are located 0.28 and 0.40 eV below HOMO. Moreover, in agreement with the proposed $A_{Ac}2$ mechanism, the most reactive site belongs to O_{14}, and O_{12} makes more contributions to LUMO (Fig. 3).

On the other hand, the charge distribution and the energy of LUMO can be indicative of the carcinogenic activity of a substance, according to Leão and Pavão (1997); they indicated that the carcinogens have a low LUMO energy. In the case of the aflatoxin B1 compound, the LUMO has a considerable lower absolute energy, −2.38 eV, and it shows the main contributions around the C_{11} atom, which is the region of interest.

Hydrolysis of Aflatoxin B1

Coming back to the aflatoxin B1 ground-state structure (see Fig. 1b), the relatively longer O_{10}−C_{11} distance, 1.423 Å, as compared with the O_{10}−C_{9c} bond length, 1.354 Å, is consistent with the feature that the O_{10} atom may cause rupture of the O_{10}−C_{11} bond, when the protonation is done just at the O_{10} site, as indicated in structure **1a** in Figs. 4 and 5 (see also Scheme 2 and Table 6). However, protonation may also occur at O_{14}, as shown in structure **1b** in Fig. 4. In both cases, the acidic medium produces hydrolysis of the lactone ring, yielding a compound that contains both hydroxylic and carboxylic groups, **1h**. In more detail, in the first step of the reaction mechanism (stereoisomer **1: a → b)** (see Fig. 4), our calculations indicate that proton addition occurs between the O_{10} and the O_{14} atoms, but closer to O_{10}, yielding a TS which has an imaginary frequency at 1489 cm^{-1}), with vector displacements around the O_{10}−H−O_{14} atoms; **1b**. The O_{14}−H and O_{10}−H contacts in **1b** show distances of 1.441 and 1.174 Å, respectively, which indicate a stronger bonding interaction for O_{10}−H. The bond lengths for C_{11}−O_{10} (1.462 Å) and

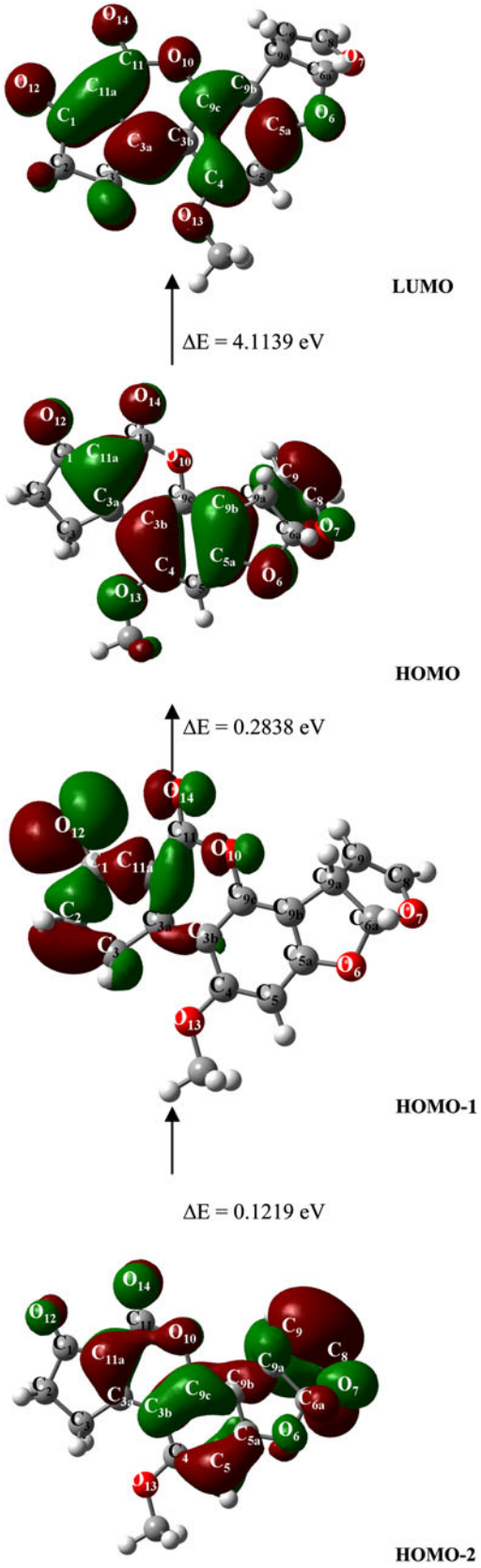

Fig. 3 LUMO, HOMO, HOMO-1, and HOMO-2 contour plots for the aflatoxin molecule (**1**) at the B3LYP/6-311+G(d,p)

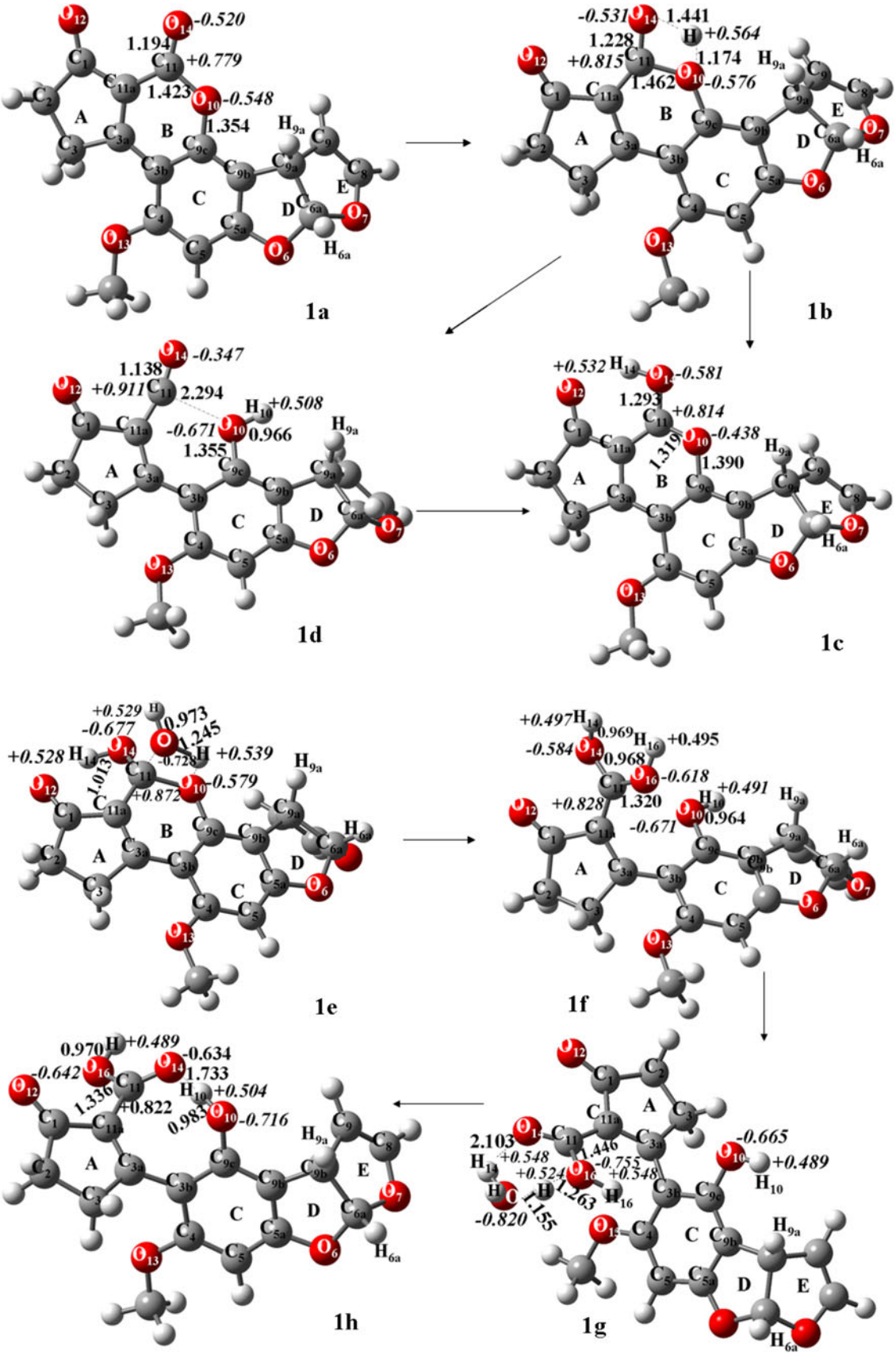

Fig. 4 Intermediates and transition states for the reaction pathway **1a** → **1h** at the B3LYP/6-311+G(d,p) level of theory for molecule **1**

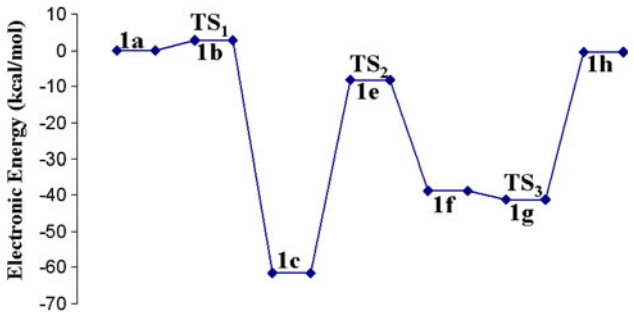

Fig. 5 Key points of the potential energy surface, at B3LYP/6-311+G(d,p), for the reaction pathway of aflatoxin B1 (**1a** → **1h**), of system **I**

$O_{10}-C_{9c}$ (1.407 Å) are rather longer than those of **1a**. Besides, for the TS **1b** the $C_{11}-O_{14}-H$ and $C_{11}-O_{10}-H$ angles were found to be 76.8° and 77.5°, whereas the $O_{14}-C_{11}-O_{10}$ angle was found to be 100.8° (slightly smaller than sp^3 hybridization). In **1a** this angle is 116.6°, revealing that the hybridization is of the sp^2 type. Furthermore, the TS **1b** may produce two intermediates, **1c** and **1d**, with the proton lying at O_{14} or at O_{10}, respectively. The results obtained suggest that the $H-O_{14}$ (**1c**) structure may originate the more favorable pathway, because it is considerably more stable, by about 25.3 kcal/mol in electronic energy, than **1d**. In fact, the reaction pathways originating from **1d** may be disregarded. The reaction pathways from TS to $O_{14}-H$ and from TS to $O_{10}-H$ structures were verified by an IRC calculation.

Then the addition of one proton produces the intermediate **1c**. The $C_{11}-O_{14}$ bond length was calculated to be 1.293 Å, which is a rather long C–O bond length, i.e., 0.099 Å longer than that of the **1a** structure of aflatoxin. The interaction of **1a** with a proton enhances the electronic delocalization of the B and C rings, as can be seen by the shortening of the C–C distances (see structure **1c** in Fig. 4). As can be observed, the $C_{11}-C_{11a}$, $C_{11}-C_{10}$, $C_{3a}-C_{3b}$, $C_{9b}-O_{9c}$, C_4-O_5, C_4-O_{13}, and $C_{5a}-O_6$ bond lengths are clearly shortened, whereas the $O_{10}-C_{9c}$, $C_{9c}-C_{3b}$,

Scheme 2 Steps proposed for the hydrolysis of aflatoxin B1 under acidic conditions

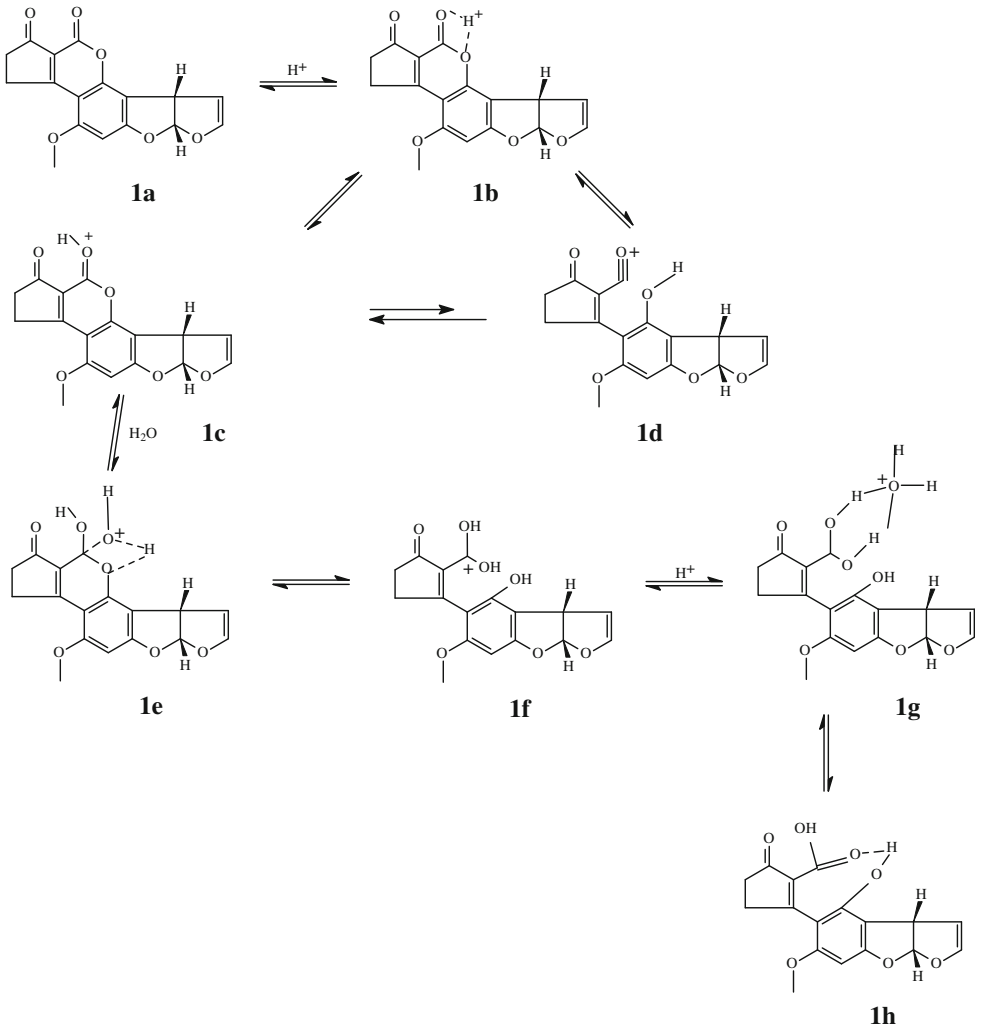

Table 6 Electronic energy (in the gas phase) for the reaction pathway of aflatoxin B1 (**1a** → **1h**) of system 1, at the levels of theory B3LYP/6-311+G(d,p)

Molecule	E_{elec}	Total energy	
		Hartrees	kcal/mol
1a	−1106.6454		
H_3O^+	−76.7311		
1a + H_3O^+ = **I**		−1183.3765	0.0000
1b	−1106.9138		
H_2O	−76.4585		
1b + H_2O = **II**		−1183.3722	
Difference, **II** − **I**		0.0042	2.6382
1c	−1107.0157		
1c + H_2O = **III**		−1183.4742	
Difference, **III** − **I**		−0.0977	−61.3077
1e (**IV**)	−1183.3895		
Difference, **IV** − **I**		−0.0130	−8.1769
1f (**V**)	−1183.4381		
Difference, **V** – **I**		−0.0616	−38.6658
1g	−1259.9003		
1g–H_2O (**VI**)		−1183.4418	
Difference, **VI** – **I**		−0.0654	−41.0332
H_2O–H_3O^+ (**VII**)		−0.2726	
1h	−1183.1048		
1h + **VII** = **VIII**		−1183.3774	
Difference, **VIII** – **I**		−0.0009	−0.5783

C_{3a}−C_{11a}, C_4−C_{3b}, and C_{9b}−C_{5a} distances are lengthened with respect to the ground state.

The interaction of a proton with O_{14} affects, first, the net charge distribution of the C_{11}−O_{14} bond. The O_{14} atom becomes more negative, while the charge on C_{11} also becomes positively charged. This interaction enhances the electrophilicity of the carbon atom C_{11}. The C_{11} charge in **1c** is more positive, by 0.035 e^-, than that of **1a**. Another notorious phenomenon in **1c** is the charge distribution for some carbon atoms of the aromatic ring B. Two of them, O_{10} and C_{3b}, increase their positivite character by 0.110 and 0.047 e^- respectively, while C_{9c} and C_{11a} become more negative (0.103 and 0.037 atomic charge unit).

Further, our results also indicate that the lactonic ring may also be broken at the O_{10}−C_{11} bond, producing a $C_{11} \equiv O_{14}$ acylium ion as an intermediate, which is recognized in structure **1d**, located 25.3 kcal/mol above **1c** (relative electronic energy). It is worth noting that this intermediate can be stabilized by resonance (Boer 1968; Olah and Westerman 1973), which is in agreement with the theoretical calculations for the $C_{11} \equiv O_{14}$ distance; the result obtained, 1.138 Å, indicates a strong bond formation.

Also, a TS called TS2 (imaginary frequency, 1497 cm^{-1}), **1e**, is suggested before the final product, **1h**. The addition of one water molecule produced the intermediate **1f**. The C_{11}−O_{14} distance was calculated to be 1.309 Å, indicating a rather long C–O bond. Similarly, the C_{11}−O_{14} bond is longer, by 0.115 Å, than **1a**. Also, the interaction of **1c** with the H_2O molecule produces an increase in the electronic delocalization in ring C, which includes the contributions of the C_{3a}, C_{11a}, C_1, and O_{12} sites of **1f**. As shown in Fig. 4, the C_{11}−O_{10}, C_{11a}−C_{3a}, C_{3b}−C_4, C_{5a}−C_{9b}, and C_{9c}−O_{10} distances are lengthened. To a minor extent, the C_{3a}−C_{3b}, C_4−C_5, C_5−C_{5a}, C_{11}−C_{11a}, and C_{9b}−C_{9c} bond lengths are shortened, with respect to **1a**. The interaction of one water molecule with the C_{11} atom affects, first, the net charges of the C_{11}−O_{14} bond. The O_{14} atom becomes more negative, and the charge on C_{11} is more positive, by 0.049 e^-, than the corresponding value for **1a**. Besides, others atoms of the B ring suffer changes in the charge distribution. Two of them, C_{3a} (0.106 e^-) and C_{3b} (0.009 e^-; 0.589) increases their positive charges with respect to **1a**, while C_{9c}, C_{11a}, and O_{10} become more negative (0.033 and 0.123 atomic charge units).

A **1g** TS, TS3 (imaginary frequency, 282.6 cm^{-1}), is suggested before the final product, **1h,** is formed. Abstraction of the proton from the oxygen atom provokes changes in the O_{16}−C_{11}, C_{11}−O_{14}, and C_{3a}−C_{3b} distances that are clearly reflected in the lengthening of these bond lengths. In addition, C_{3a}−C_{11a} showed a shortening of the distance (by 0.013 Å). All bond lengths and bond angles in the ring B of structure **1g** change considerably and affects those of rings A and C, with respect to **1f**. At the same time, planarity of ring A is absent, since the $C_3C_{3a}C_{3b}C_{9c}$ and $C_{11a}C_{3a}C_{3b}C_4$ dihedral angles are −55.4° and 61.5°, respectively. As for the electronic details, the O_{14} and C_{11} atoms of **1g** become positively and negatively charged, by 0.046 e^- and 0.003 e^-, respectively, compared to the corresponding value for **1f**.

The hydrolysis of the aflatoxin B1 molecule originates two conformers as final products. Figure 4 shows the final product, **1h**. These two species can occur with or without the formation of an intramolecular hydrogen bond. In fact, in **1h** an O_{10}−H−O_{14} bonding is formed, with the relatively short H−O_{14} distance of 1.733 Å. Around the H−bond region, the C_{11a}−C_{3a}, C_{11}−O_{16}, and C_{9c}−O_{10} distances are shortened, and the C_{11}−O_{14} and O_{10}−H_{10} bonds are lengthened.

It should be noted that the H-bond formation stabilizes structure **1h**, by about 7.4 kcal/mol (relative electronic energy). This result is indicative of considerable bond strength for this bond and exemplifies the importance of this type ofn bonding on the stability of this conformer**.** It is important to mention that the generality of this analysis is in complete agreement with a hydrolytic mechanism for the lactone (a cyclic ester) compound, belonging to the class of

acid-catalyzed, acyl cleavage, second-order reactions ($A_{AC}2$) (Zimmermann and Rudolph 1965), as proposed by Ingold.

In this sense, it is convenient to note that, to classify the catalytic hydrolysis of esters, eight possible mechanisms have been proposed, the most common being $B_{AC}2$ for basic conditions and $A_{AC}2$ for acid catalysis. The above notations (Sykes 1986) indicate that the O–R bond of the acyl group is commonly broken by a bimolecular procedure. Consequently, the lactone ring of aflatoxin B1 must be broken by means of an $A_{AC}2$ mechanism under diluted acid conditions. In this mechanism, the ester first accepts a proton at the carbonyl oxygen and this change enhances the positive charge on the carbonyl carbon. This protonation facilitates the successive addition of water at that position to form a tetrahedral intermediate, consisting of the protonated cyclic ester and water.

Fluorescence of Aflatoxin B1

The molecular structure is one of the most important features in fluorescent species. The dihedral angles for the ground-state structure of aflatoxin B1 are reported in Table 3. These results indicate that the A, B, C, and D rings show a planar conformation, with all dihedral angles varying by less than 1° from planarity, whereas the E ring is located outside that plane. Particularly, the coplanarity of the phenyl C ring with the B one promotes some degree of conjugation, enabling the formation of an extended π system on these rings, which in turn yields an efficient absorption of relatively low-energy photons.

Due to planarity, the degree of rotational freedom is notably restricted and thus the rotational-vibrational relaxation mechanism does not contribute to the loss of the absorbed energy. As a result, the singlet–triplet excitation, with the associated emission for returning to the ground state, is the main fluorescence mechanism for relieving the energy excess, yielding a molecule with high fluorescence quantum yields.

In the singlet state, the B3LYP/6-31G(d,p) time-dependent results (see Table 7) indicate that the lowest excitation occurs at 377 nm but with a zero value for the oscillator strength (f). On the contrary, the singlet excitation occurring at 309 nm (4.01 eV) shows the highest f value (0.24) and represents a HOMO(-2)-LUMO transition; these results are in agreement with the reported values (Guedes and Ericsson 2006). Note that the use of B3LYP/6-31+G(d,p) for this single excitation renders a value of 312 nm (3.96 eV), with an oscillator strength of 0.23, which is in agreement with a previously reported value, (Bauernschmitt and Ahlrichs 1996).

For the triplet state the B3LYP/6-31G(d,p) results indicate 408 nm for the main transition, with an f value of 0.32 and representing predominantly a HOMO-LUMO(+2) event, which is in reasonable agreement with the experimental value of 425 nm (Purchase 1974). Note that this wavelength falls in the visible region. It is to be mentioned that use of the larger 6-311+G(d,p) basis set yields 433 nm for this transition, in better concordance with the experiment. A similar value, 431 nm was obtained using the 6-31+G(d,p) basis set for the transition estimation, which takes as input a 631G(d,p) optimized geometry.

Table 7 Absorption spectra determining vertical electronic excitations from the ground state using the TD-DFT with B3LYP/6-31G(d,p)

Excited state		Excitation energy (nm)	Oscillator strength (f)
1	Triplet	466.98	0.0000
2	Triplet	416.60	0.0000
3	Singlet	376.86	0.0000
4	Triplet	362.85	0.0000
5	Singlet	332.61	0.1721
6	Triplet	323.38	0.0000
7	Triplet	311.10	0.0000
8	Singlet	309.01	0.2366
9	Triplet	307.00	0.0000

Conclusions

The aflatoxin B1 compound was studied by means of DFT; the determined structural and electronic properties allow the characterization of its reactivity behavior in acidic hydrolysis. It was suggested that the reaction pathway that involves the lactone ring is the main one responsible of this process. The results obtained agree with the experimental findings for this type of hydrolysis. It was found that the B ring is broken completely during the reaction mechanism, producing transference of charge for the ground state structure **1**, and the excited singlet indicated the ability of the molecule to display fluorescence. These fluorescence properties are lost when the planarity of the molecule is broken, namely, by hydrolysis under acidic conditions and opening of the lactonic ring. The atomic charges, electrostatic potential, and HOMO and LUMO indicate that the oxygen atom O_{14} is the more fitting site of the aflatoxin moiety for interaction with protons, generated from the aqueous citric acid conditions. Thus, it was shown that the lactonic ring is hydrolyzed under acidic conditions by an acid-acyl bimolecular mechanism ($A_{AC}2$), implying the deletion of its carcinogenic properties.

Acknowledgments We acknowledge financial support from DGAPA-UNAM under Projects PAPIME (PE201905), CONACyT-México,

and PACIVE (VIASC-103, FESC-UNAM). Access to the Kan-Balam supercomputer at DGSCA-UNAM is greatly appreciated. We also truly appreciate the valuable discussions with Dra. Rocío Cartas, Dr. Gustavo Rivera, and Dr. Victor Chávez.

References

Applebaum RS, Marth EH (1982) Inactivation of aflatoxin M_1 in milk using hydrogen peroxide and hydrogen peroxide plus riboflavin or lactoperoxidase. J Food Prot 45:557–560

Asao T, Buchi G, Abdel-Kader MM, Chang SB, Wick EL, Wogan GN (1963) Aflatoxins B and G. J Am Chem Soc 85:1706–1707

Bauernschmitt R, Ahlrichs R (1996) Treatment of electronic excitations within the adiabatic approximation of time dependent density functional theory. Chem Phys Lett 256:454–464

Becke AD (1988) Density-functional exchange-energy approximation with correct asymptotic behavior. Phys Rev A 38:3098–3100

Becke AD (1993) Density-functional thermochemistry. III. The role of exact exchange. J Chem Phys 98:5648–5652

Billes F, Móricz AM, Tyihák E, Mikosch H (2006) Simulated vibrational spectra of aflatoxins and their demethylated products and the estimation of the energies of the demethylation reactions. Spectrochim Acta A 64:600–622

Boer FP (1968) The crystal structure of a Friedel-Crafts intermediate. Methyloxocarbonium hexafluoroantimonate. J Am Chem Soc 90:6706–6710

Brekke OL, Stringfellow AC, Peplinski AJ (1978) Aflatoxin inactivation in corn by ammonia gas: laboratory trials. J Agric Food Chem 25:1383

Bren U, Guengerich FP, Mavri J (2007) Guanine alkylation by the potent carcinogen aflatoxin B1: quantum chemical calculations. Chem Res Toxicol 20:1134–1140

Buchi G, Foulkes DM, Kurono M, Mitchell GF, Schneider RS (1967) The total synthesis of racemic aflatoxin B_1. J Am Chem Soc 89:6745–6753

Cater CM, Rhee KC, Hagenmaier RD, Mattil KF (1974) Aqueous extraction—an alternative oilseed milling process. J Am Oil Chem Soc 51:137–141

Clark T, Chandrasekhar J, Spitznagel GW, Schleyer PVR (1983) Efficient diffuse function-augmented basis sets for anion calculations. III. The 3–21+G basis set for first-row elements, Li-F. J Comput Chem 4:294–301

Deppmeier BJ, Driessen AJ, Hehre TS, Hehre WJ, Johnson JA, Klunzinger PE, Leonard JM, Pham IN, Pietro WJ, Jianguo Yu, Kong J, White CA, Krylov AI, Sherrill CD, Adamson RD, Furlani TR, Lee MS, Lee AM, Gwaltney SR, Adams TR, Ochsenfeld C, Gilbert ATB, Kedziora GS, Rassolov VA, Maurice DR, Nair N, Shao Y, Besley NA, Maslen PE, Dombroski JP, Dachsel H, Zhang WM, Korambath PP, Baker J, Byrd EFC, Van Voorhis T, Oumi M, Hirata S, Hsu CP, Ishikawa N, Florian J, Warshel A, Johnson BG, Gill PMW, Head-Gordon M, Pople JA (2002) SPARTAN '02. Wavefunction, Inc., Irvine, CA

Dewar MJS, Zoebisch EG, Healy EF, Stewart JJP (1985) AM1: a new general purpose quantum mechanical molecular model. J Am Chem Soc 107:3902–3909

Dollear FG, Mann GE, Codifer LP, Gardner HK, Koltun SP, Vix HLE (1968) Elimination of aflatoxins from peanut meal. J Am Oil Chem Soc 45:862–865

Doyle MP, Marth EH (1978a) Bisulfite degrades aflatoxin: effect of citric acid and methanol and possible mechanism of degradation. J Food Prot 41:774–780

Doyle MP, Marth EH (1978b) Bisulfite degrades aflatoxin: effect of temperature and concentration of bisulfite. J Food Prot 41:891–896

Dutton MF, Heathcote JG (1968) The structure, biochemical properties and origin of aflatoxins B_{2a} and G_{2a}. Chem Ind 13:418–421

Frisch MJ, Pople JA, Binkley JS (1984) Self-consistent molecular orbital methods 25. Supplementary functions for Gaussian basis sets. J Chem Phys 80:3265–3269

Frisch MJ, Trucks GW, Schlegel HB, Scuseria GE, Robb MA, Cheeseman JR, Zakrzewski VG, Montgomery JA Jr, Vreven T, Kudin KN, Burant JC, Millan JM, Iyengar SS, Tomasi J, Barone V, Mennucci B, Cossi M, Scalmani G, Rega N, Petersson GA, Nakatsuji H, Hada M, Ehara M, Toyota K, Fukuda R, Hasegawa J, Ishida M, Nakajima T, Honda Y, Kitao O, Nakai H, Klene M, Li X, Knox JE, Hratchian HP, Cross JB, Adamo C, Jaramillo J, Gomperts R, Stratmann RE, Yazyev O, Austin AJ, Cammi R, Pomelli C, Ochterski JW, Ayala PY, Morokuma K, Voth GA, Salvador P, Dannenberg JJ, Zakrzewski VG, Dapprich S, Daniels AD, Strain MC, Farkas O, Malick DK, Rabuck AD, Raghavachari K, Foresman JB, Ortiz JV, Cui Q, Baboul AG, Clifford S, Cioslowski J, Stefanov BB, Liu G, Liashenko A, Piskorz P, Komaromi I, Martin RL, Fox DJ, Keith T, Al-Laham MA, Peng CY, Nanayakkara A, Challacombe M, Gill PMW, Johnson B, Chen W, Wong MW, Gonzalez C, Pople JA (2003) Gaussian 03, revision B.03. Gaussian, Inc., Pittsburgh, PA

Guedes RC, Ericsson LA (2006) Theoretical characterization of aflatoxins and their phototoxic reactions. Chem Phys Lett 42:328–333

Hagler WM, Hutchins JE, Hamilton PB (1982) Destruction of aflatoxin in corn with sodium bisulfite. J Food Prot 45:1287–1291

Hagler WM, Hutchins JE, Hamilton PB (1983) Destruction of aflatoxin in corn with sodium bisulfite: isolation of the major product aflatoxin B_1. J Food Prot 46:295–298

Hariharan PC, Pople JA (1973) The influence of polarization functions on molecular orbital hydrogenation energies. Theor Chim Acta 28:213–222

International Agency for Research on Cancer (IARC) (1987) IARC monograph on the evaluation of carcinogenic risk to humans. IARC, Lyon, Suppl 1, pp 82–87

Leão MBC, Pavão AC (1997) Molecular orbital analysis of chemical carcinogens. Int J Quant Chem 62:323–328

Lee LS, Dunn JJ, DeLucca AJ, Ciegler A (1981) Role of lactone ring of aflatoxin B1 in toxicity and mutagenicity. Experientia 37:16–17

Lee C, Yang W, Parr RG (1988) Development of the Colle-Salvetti correlation-energy formula into a functional of the electron density. Phys Rev B 37:785–789

Maitra NT, Tempel DG (2006) Long-range excitations in time-dependent density functional theory. J Chem Phys 125:184111–184116

Mann GE, Codifer LP, Garner HK, Koltun SP, Dollear FG (1970) Chemical inactivation of aflatoxins in peanut and cottonseed meals. J Am Oil Chem Soc 47:173–176

Mayer I (1986a) On bond orders and valences in the Ab initio quantum chemical theory. Int J Quant Chem 29:73–84

Mayer I (1986b) Bond orders and valences from ab initio wave functions. Int J Quant Chem 29:477–483

McKenzie KS, Sarr AB, Mayura K, Bailey RH, Millar DR, Rogers TD, Corred WP, Voss KA, Plattner RD, Kubena LF, Phillips TD (1997) Oxidative degradation and detoxification of mycotoxins using a novel source of ozone. Food Chem Toxicol 35:807–820

McKenzie KS, Kubena LE, Denvir AJ, Rogers TD, Hitchens GD, Bailey RH, Harvey RB, Buckley SA, Phillips TD (1998) Aflatoxicosis in turkey poults is prevented by treatment of

naturally contaminated corn with ozone generated by electrolysis. Poultry Sci 77:1094–1102

Méndez-Albores A, Arámbula-Villa G, Loarca-Piña MGF, Castaño-Tostado E, Moreno-Martínez E (2005) Safety and efficacy evaluation of aqueous citric acid to degrade B-aflatoxins in maize. Food Chem Toxicol 43:233–238

Méndez-Albores A, Del Río-García JC, Moreno-Martínez E (2007) Decontamination of aflatoxin duckling feed with aqueous citric acid treatment. Anim Feed Sci Technol 135:249–262

Méndez-Albores A, Nicolás Vázquez I, Miranda-Ruvalcaba R, Moreno-Martínez E (2008) Mass spectrometry/mass spectrometry study on the degradation of B-aflatoxins in maize with aqueous citric acid. Am J Agric Biol Sci 3:482–489

Mercado CJ, Real MPN, Del Rosario RR (1991) Chemical detoxification of aflatoxin-containing copra. J Food Sci 56:733–735

Moerck KE, McElfresh P, Wohlman A, Hilton BW (1980) Aflatoxin destruction in corn using sodium bisulfite, sodium hydroxide and aqueous ammonia. J Food Prot 43:571–574

Murray JS, Politzer P (1998) Statistical analysis of the molecular surface electrostatic potential: an approach to describing noncovalent interactions in condensed phases. J Mol Struct (Theochem) 425:107–114

Murray JS, Abu-Awwad F, Politzer P, Wilson LC, Troupin AS, Wall RE (1998) Molecular surface electrostatic potentials of anticonvulsant drugs. Int J Quant Chem 70:1137–1143

Murray JS, Peralta-Inga Z, Politzer P (1999) Conformational dependence of molecular surface electrostatic potentials. Int J Quant Chem 75:267–273

Okajima T, Hashikawa A (2000) Ab initio MO study on the difference of solvent effect between exo and endo stereoisomers of aflatoxin B1 8, 9-oxide for SN2 type nucleophilic ring opening. J Mol Struct (Theochem) 532:205–212

Olah GA, Westerman PW (1973) Stable carbocations. CXLIV. The structure of benzoyl cations based on their carbon-13 nuclear magnetic resonance spectroscopic study. The importance of delocalized, "ketene-like" carbenium ion resonance forms. J Am Chem Soc 95:3706–3709

Pachter R, Steyn PS (1985) Quantum-chemical studies of aflatoxin B1, sterigmatocystin and versicolorin A, and a comparison with their mutagenic activity. Mutat Res 143:87–91

Park DL, Jemmali M, Frayssinet C, LaFarge-Frayssinet C, Yvon M (1981) Decontamination of aflatoxin-containing peanut meal using monomethylamine:$Ca(OH)_2$. J Am Oil Chem Soc 58:994–997

Park DL, Lee LS, Koltun SA (1984) Distribution of ammonia-related aflatoxin reaction products in cottonseed meal. J Am Oil Chem Soc 61:1071–1074

Park DL, Lee LS, Price RL, Pohland AE (1988) Review of the decontamination of aflatoxins by ammoniation: current status and regulation. J Assoc Off Anal Chem 71:685–703

Pavão AC, Soares Neto LA, Ferreira Neto J, Leão MBC (1995) Structure and activity of aflatoxins B and G. J Mol Struct (Theochem) 337:57–60

Purchase IFH (1974) Aflatoxin. In: Butler WH (ed) Mycotoxins. Elsevier, Amsterdam, pp 1–4

Ramírez-Galicia G, Garduño-Juárez R, Vargas MG (2007) Effect of water molecules on the fluorescence enhancement of aflatoxin B1 mediated by aflatoxin B1: β-cyclodextrin complexes. A theoretical study. Photochem Photobiol Sci 6:110–118

Reed AE, Weinstock RB, Weinhold F (1985) Natural-population analysis. J Chem Phys 83:735–746

Samarajeewa U, Sen AC, Fernando SY, Ahmed EM, Wei CI (1991) Inactivation of aflatoxin B_1 in corn meal, copra meal and peanuts by chlorine gas treatment. Food Chem Toxicol 29:41–47

Stratmann RE, Scuseria GE, Frisch MJ (1998) An efficient implementation of time-dependent density-functional theory for the calculation of excitation. J Chem Phys 109:8218–8224

Sykes PA (1986) Guidebook to mechanism in organic chemistry, 6a edn. Longman Scientific & Technical, New York, pp 240–244

van Soest TC, Peerdeman AF (1970a) The crystal structures of aflatoxinB_1. I. The structure of the chloroform solvate of aflatoxin B_1 and the absolute configuration of aflatoxin B_1. Acta Crystallogr B26:1940–1947

van Soest TC, Peerdeman AF (1970b) The crystal structures of aflatoxin B_1. II. The structure of an orthorhombic and a monoclinic modification. Acta Crystallogr B26:1947–1955

Yiannikouris A, André G, Poughon L, François J, Dussap CG, Jeminet G, Bertin G, Jouany JP (2006) Chemical and conformational study of the interactions involved in mycotoxin complexation with D-glucans. Biomacromolecules 7:1147–1155

Zimmermann H, Rudolph J (1965) Protonic states and the mechanism of acid-catalysed esterification. Angew Chem Int Ed Engl 4: 40–49